Spatiotemporal Characteristics and Climate Influences on Marine Heatwaves in the Maluku Sea (1996–2025)

La Ode Ashamad Nusriah[a], Syahrajad Al Syarqiyah[a], Yahya Darmawan[b,*]
[a]Meteorology Study Program, Sekolah Tinggi Meteorologi Klimatologi dan Geofisika, Tangerang, Indonesia
[b]Climatology Study Program, Sekolah Tinggi Meteorologi Klimatologi dan Geofisika, Tangerang, Indonesia
*Corresponding author: yahya.darmawan@bmkg.go.id

Abstract: Marine heatwaves (MHWs) threaten marine ecosystems, yet long-term MHW characteristics in the Maluku Sea, a strategic area along the Indonesian Throughflow pathway, remain poorly documented. This study analyzes the spatiotemporal characteristics of MHWs during 1996–2025 from daily NOAA OISST v2.1 data and assesses their statistical associations with the El Niño–Southern Oscillation (ENSO) and monsoon variability. MHWs were detected following Hobday et al. (90th percentile, 11-day window, minimum duration of five days). MHW frequency (+0.82 events year^{-1} decade^{-1}) and duration (+1.8 days decade^{-1}) increased significantly (modified Mann–Kendall, $p < 0.05$), whereas maximum intensity decreased (−0.09 °C decade^{-1}); these trends are relative to a 1996–2025 baseline in a basin that warmed by 0.26 °C decade^{-1}. ENSO showed a stronger association with monthly MHW frequency than the monsoon index examined (lag 0: $r = -0.29$, $p = 0.002$), with more MHWs during La Niña; the monsoon association was not significant after controlling for ENSO. Together they explain less than 9% of the variance, so unexamined processes, including the Indian Ocean Dipole and ocean dynamics, remain important.

Keywords: ENSO; marine heatwaves; Maluku Sea; monsoon; remote sensing; sea surface temperature

I. INTRODUCTION

Marine heatwaves (MHWs) are discrete periods in which sea surface temperature (SST) exceeds a seasonally varying 90th-percentile threshold for at least five consecutive days [1]. They have become longer and more frequent over the past century [2] and threaten coral reefs, fisheries and other marine ecosystem services. Recent anomalous ocean warming in Southeast Asian waters, such as the 2023 event linked to El Niño [3], underlines the need for regional MHW characterization based on long satellite SST records [4].

The Maluku Sea (123°–132°E, 6°S–6°N) lies in the eastern Indonesian maritime continent along the pathway of the Indonesian Throughflow (ITF, Arlindo), which carries warm Pacific water and heat to the Indian Ocean [5]–[7]. Its SST is influenced by interannual ENSO variability and the seasonal Asian–Australian monsoon [8], which makes the region a useful test case for how extreme ocean heat responds to large-scale climate variability [5].

Previous MHW studies in Indonesian waters report spatially variable results [9]. South of West Java, long-term variability was dominated by extreme ENSO years such as 1998, 2010 and 2016 [9]. In the Banda Sea, monsoon wind variability was reported as the strongest correlate of MHW frequency, with a weak and indirect ENSO relationship [10]. These contrasting results suggest that climate–MHW relationships in Indonesian seas depend on local circulation and geographic setting [11].

However, long-term investigations of MHW characteristics and the relative roles of ENSO and monsoon variability in the Maluku Sea remain limited, despite the region's strategic position within the ITF pathway [5], [12]. Because the Maluku Sea lies upstream of the Banda Sea [13], it is unclear whether the monsoon-dominated pattern reported downstream [10] also applies here.

This study contributes (i) a 30-year characterization of MHW frequency, duration and intensity in the Maluku Sea from daily OISST v2.1; (ii) a spatial and temporal analysis with autocorrelation-aware trend tests and false-discovery-rate control; (iii) an assessment of ENSO and monsoon associations with MHW frequency, including a statistically supported tendency toward more MHWs during La Niña; and (iv) ERA5 wind and surface heat flux composites used to evaluate whether local atmospheric forcing is consistent with that tendency.

The objective is to characterize the spatiotemporal variability of MHW frequency, duration and intensity in the Maluku Sea during 1996–2025 and to assess the relative statistical associations of ENSO and monsoon variability with MHW frequency. Results are interpreted as associations and not as causal attribution.

II. METHODOLOGY

2.1 Study Area

This study focuses on the Maluku Sea, located in the eastern Indonesian maritime continent, covering the geographic domain of 123°–132°E and 6°S–6°N (Figure 1). The Maluku Sea is an important oceanographic region located along the pathway of the Indonesian Throughflow (ITF), which contributes to heat exchange between the Pacific and Indian Oceans [5], [6]. Sea surface temperature

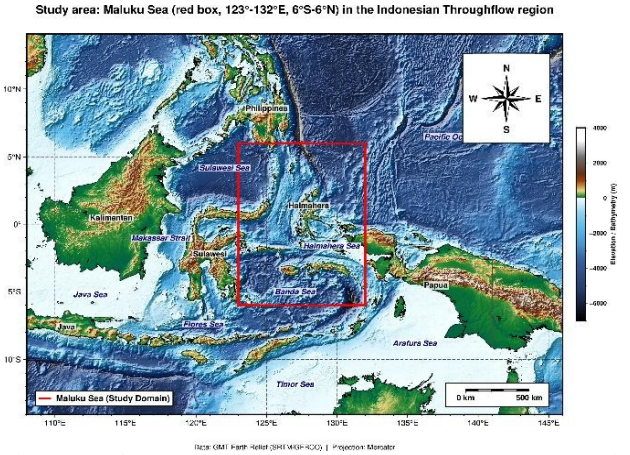


Figure 1. Study area: the Maluku Sea (red box, 123°–132°E, 6°S–6°N) in the Indonesian Throughflow region.

(SST) variability in this region is strongly influenced by large-scale climate modes, including El Niño–Southern Oscillation (ENSO) and the Asian–Australian monsoon system [8], [14], making it an important region for investigating marine heatwave (MHW) variability.

2.2 Data

Daily SST was obtained from the NOAA Optimum Interpolation SST version 2.1 (OISST v2.1, also called DOISST), a 0.25° daily product that blends AVHRR satellite and in situ observations [15]–[17]. The record spans 1 January 1996 to 31 December 2025 (10,958 days); the subset 123°–132°E, 6°S–6°N contains 1,715 ocean grid cells. Six missing days (0.055%) were filled by linear interpolation (maximum gap of three days). The 30-year length meets the minimum recommended for MHW climatologies [1] and the WMO climate-normal period [18], and includes the El Niño episodes of 1997/98, 2009/10 and 2015/16 [9].

ENSO was represented by the monthly Niño3.4 SST anomaly from NOAA CPC. Monsoon variability was represented by the Australian Monsoon Index (AUSMI) of Kajikawa et al. [19], defined as the area-mean 850-hPa zonal wind (U850) anomaly over 5°–15°S, 110°–130°E, computed from ERA5 [20] as the monthly anomaly relative to the 1996–2025 monthly climatology; positive values denote stronger low-level westerlies (a stronger west/summer monsoon). Because this domain lies mostly south of the study area (6°S–6°N), the index is a large-scale proxy and not a local wind measure. For the heat-flux analysis, monthly 10-m wind speed (from U10 and V10) and the surface fluxes SSR, STR, SLHF and SSHF were taken from ERA5 at 0.25° [20]. Accumulated fluxes were converted to W m^{-2} by dividing by 3600 s, and net surface heat flux was Qnet = SSR + STR + SLHF + SSHF, positive downward. Absolute flux magnitudes depend on the ERA5 sampling and unit conversion, so only anomalies are interpreted. Dataset details are listed in Table 1.

Table 1. Datasets used in this study.

Dataset (source)	Variable, unit, resolution	Period and preprocessing
NOAA OISST v2.1 (NOAA NCEI/PSL)	SST, °C; 0.25°; daily	1996–2025; subset 123°–132°E, 6°S–6°N; ocean mask; 6 missing days interpolated
Niño3.4 index (NOAA CPC)	SST anomaly, °C; 5°N–5°S, 170°–120°W; monthly	1996–2025; ONI-type phases (3-month mean, ≥ 5 seasons)
AUSMI from ERA5 U850 (C3S/CDS), 5°–15°S, 110°–130°E	850-hPa zonal wind anomaly, m s^{-1}; monthly	1996–2025; area mean; monthly anomaly
ERA5 reanalysis (C3S/CDS)	U10, V10, m s^{-1}; SSR, STR, SLHF, SSHF, W m^{-2}; 0.25°	1996–2025; monthly means; ocean mask; Qnet downward positive

All analyses were performed in Python 3.13 on Google Colaboratory using xarray 2025.12 (gridded data), NumPy 2.1 and pandas 2.2 (array and time-series operations), SciPy 1.16 (Theil–Sen slope, Pearson and Spearman correlation, Shapiro–Wilk test), pymannkendall 1.4 (original and Hamed–Rao modified Mann–Kendall tests), statsmodels 0.15 (OLS with HAC errors and Benjamini–Hochberg FDR correction), and Matplotlib 3.10 with Cartopy 0.26 (maps). Code is available from the corresponding author on request.

2.3 Marine Heatwave Detection

MHW events were identified following the standard threshold-based approach of [1], which has been widely applied in both global and regional MHW studies [1], [2], [9]. In this framework, an MHW is defined as a discrete period during which daily SST exceeds the seasonally varying 90th percentile climatological threshold for a minimum of five consecutive days:

$$SST(t) > SST_{\text{thr}}(d) \quad (1)$$

The daily climatology was computed for each calendar day over the 1996–2025 baseline, pooling all values within ±5 days (an 11-day window) across the 30 years, and was smoothed with a 31-day moving average, following [1]. A 366-day calendar was used so that 29 February is handled consistently in leap years, and days with missing values were ignored by the percentile and mean calculations. The baseline coincides with the study period, which fixes the threshold to the 1996–2025 climate; trends in frequency and duration are therefore relative to this baseline and partly reflect background SST warming (Section 3.2). Results are not directly comparable to studies using earlier baselines such as 1982–2011 [21]:

$$SST(d) = \frac{1}{11}\sum_{i=-5}^{5} S\,ST(d+i) \quad (2)$$

The 90th percentile threshold was then derived from the same pooled 11-day sample for each day of year and smoothed in the same way. The threshold is used only for detection; event intensity is measured against the climatology.

$$SST_{\text{thr}}(d) = P_{90}\big(SST(d)\big) \quad (3)$$

Detection followed the order of [1]: exceedance runs of at least five consecutive days were identified first, and runs separated by a gap of two days or fewer were then merged into a single event (maximum gap = 2 days). Event duration includes the gap days. Detection was performed independently at each ocean grid cell.

2.4 Marine Heatwave Metrics

Detection used daily SST. Event metrics were then aggregated to annual values (trends, annual correlations, maps) and, for lagged correlation, regression and composites, to monthly values, with lags expressed in months. Aggregation keeps event-scale information because MHW days and cumulative intensity are accumulated from daily data. Domain averages use ocean cells only; duration and intensity are event-weighted means. Metrics follow [1], [4], [21], [22]:

- Frequency: number of events starting in a year (or month) per ocean grid cell (events year^{-1})
- Duration: days from the start to the end of an event, including gap days (days event^{-1})
- MHW days: total number of days per year that fall within events (days year^{-1})
- Mean and maximum intensity: mean and maximum of the SST anomaly relative to the smoothed daily climatology during an event, I(t) = SST(t) − SSTclim(d) (°C). Maximum intensity is averaged over all events in a year:

$$I(t) = SST(t) - SST_{\text{clim}}(d) \quad (4)$$

Cumulative intensity: sum of I(t) over the duration of an event (°C day):

$$I_{\text{cum}} = \sum_{t=1}^{D} I\,(t), \quad t = 1,2,\dots,D \quad (5)$$

Annual maximum intensity is the largest I(t) reached by any event in a given year. Intensity measured relative to the threshold, as in some earlier studies, is lower than intensity relative to the climatology by the mean threshold–climatology difference (0.72 °C in this domain), so values should be compared only when the same definition is used.

2.5 Trend Analysis

Long-term trends of annual MHW metrics were assessed with the Hamed–Rao modified Mann–Kendall test [23], which corrects for serial autocorrelation that otherwise inflates Type I error in the original test [24], [25]; original Mann–Kendall p-values are given for comparison. The Mann–Kendall statistic S is:

$$S = \sum_{i=1}^{n-1}\sum_{j=i+1}^{n} \operatorname{sgn}\big(x_j - x_i\big) \quad (6)$$

Trend magnitude was estimated with the Theil–Sen slope estimator [26] and is expressed per decade:

$$\beta = \operatorname{median}\left(\frac{x_j - x_i}{j - i}\right) \quad (7)$$

Spatial trends were computed for each ocean cell with at least 20 valid years. Because more than 1,700 cells are tested at once, significance was controlled with the Benjamini–Hochberg false discovery rate (FDR, α = 0.05) [27]; stippling marks cells that pass. The trend in domain-mean annual SST was computed in the same way to provide context for the fixed baseline.

2.6 Climate Index Analysis

To assess associations of ENSO and monsoon variability with MHW occurrence, Pearson correlation was computed between monthly MHW frequency anomalies (monthly climatology removed; N = 360) and the Niño3.4 and AUSMI indices [28]. Series were linearly detrended in the main analysis, and non-detrended results are also reported. Because monthly series are autocorrelated, p-values use an effective sample size N_eff = N(1 − r1x r1y)/(1 + r1x r1y), where r1 is the lag-1 autocorrelation [29]; both N and N_eff are reported:

consistent (Newey–West, 12 lags) standard errors [30], [31]; R^2, adjusted R^2 and the Durbin–Watson statistic are reported:

$$Y = \beta_0 + \beta_1 X_{\mathrm{ENSO}} + \beta_2 X_{\mathrm{Monsoon}} + \varepsilon \qquad (10)$$

Composites of MHW frequency anomalies were computed for El Niño, La Niña and neutral months, classified with the NOAA ONI criterion (3-month running mean of the Niño3.4 anomaly ≥ +0.5 °C or ≤ −0.5 °C for at least five consecutive seasons). Significance was assessed with a moving-block bootstrap (6-month blocks, 1000 resamples)

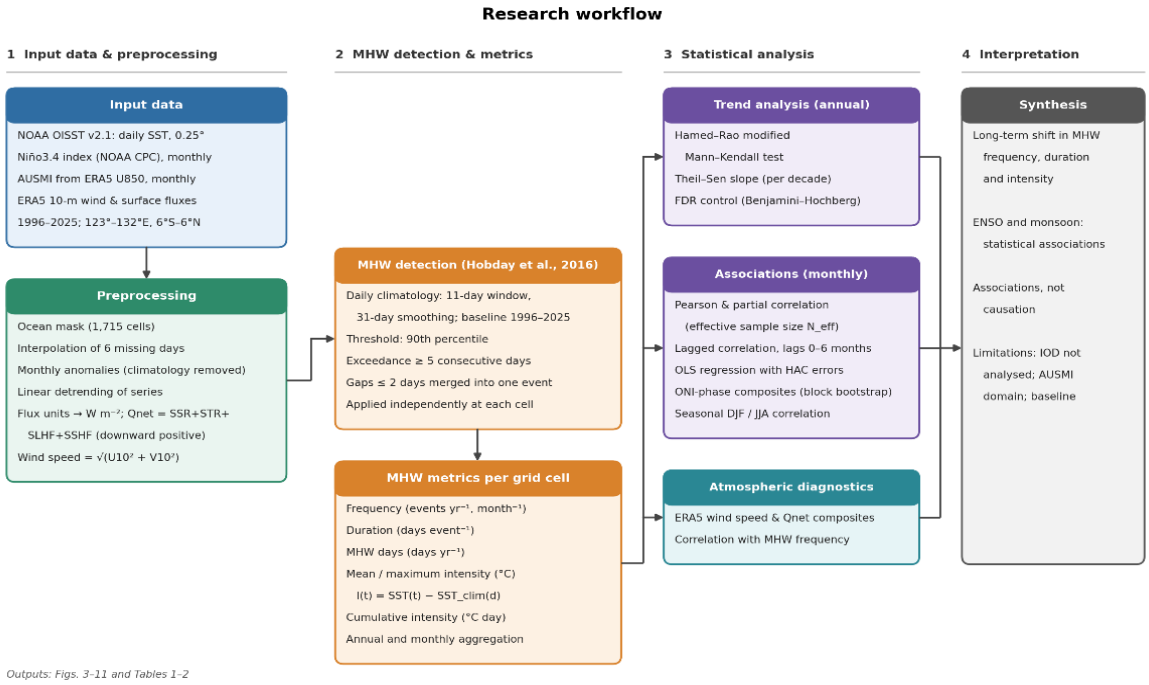


Figure 2. Flowchart of the research methodology for analyzing marine heatwave characteristics and climate influences in the Maluku Sea

$$r = \frac{\sum_{i=1}^{n}(x_i - \bar{x})\,(y_i - \bar{y})}{\sqrt{\sum_{i=1}^{n}(x_i - \bar{x})^2 \;\sum_{i=1}^{n}(y_i - \bar{y})^2}} \qquad (8)$$

Partial correlation, computed by regressing out the other index at the same lag, was used to examine the association of each index with MHW frequency while the other is held constant [28]. This describes statistical association and not causal contribution:

$$r_{xy\cdot z} = \frac{r_{xy} - r_{xz}\,r_{yz}}{\sqrt{(1 - r_{xz}^2)\left(1 - r_{yz}^2\right)}} \qquad (9)$$

A multiple linear regression of monthly MHW frequency anomalies on both indices (lag 0) was fitted by ordinary least squares with heteroskedasticity- and autocorrelation-

and FDR control. Seasonal monsoon associations were evaluated by correlating DJF and JJA mean MHW frequency in each cell with the seasonal mean AUSMI across years (n = 29–30; FDR control), and by comparing DJF and JJA frequencies with a paired Wilcoxon test.

2.7 Lagged Correlation Analysis

Lagged correlation was used to examine delayed relationships between monthly MHW frequency anomalies and the climate indices [28], [29]. The Pearson coefficient at lag τ is:

$$r(\tau) = \frac{\sum_{t=1}^{N-\tau}(X_t - \bar{X})\,(Y_{t+\tau} - \bar{Y})}{\sqrt{\sum_{t=1}^{N-\tau}(X_t - \bar{X})^2 \;\sum_{t=1}^{N-\tau}(Y_{t+\tau} - \bar{Y})^2}} \qquad (11)$$

where X_t is the climate index (Niño3.4 or AUSMI), Y_t is the monthly MHW frequency anomaly, and τ is the lag in months (positive lag: the index leads). Significance was tested with the t-statistic, with N replaced by N_eff:

$$t = \frac{r\sqrt{N-2}}{\sqrt{1-r^2}} \quad (12)$$

Lags of 0 to 6 months were examined for both indices. Because seven lags are tested per index, the best lag is interpreted against a Bonferroni-adjusted threshold ($p < 0.05/7 \approx 0.007$). Partial correlation was computed at each lag. For consistency with the annual trend analysis, an annual-scale analysis (n = 30; Pearson and Spearman) was also performed. The Indian Ocean Dipole was not included (Section 3.7). The workflow is summarized in Figure 2.

III. RESULT AND DISCUSSION

3.1 Mean Spatiotemporal Characteristics of MHWs in the Maluku Sea

Over 1996–2025, MHWs in the Maluku Sea averaged 2.03 ± 1.70 events year^{-1} per grid cell (mean ± interannual standard deviation, n = 30 years), with a mean duration of 8.80 ± 2.81 days and a mean maximum intensity of 1.20 ± 0.12 °C above the climatological mean (Figure 3); MHW days averaged 21.3 ± 22.9 days year^{-1}. Frequency varied only modestly across the basin (about 1.8–2.3 events year^{-1}), with higher values near 4–6°N, 124–125°E, west of Halmahera and in parts of the south (Figure 3a). Maximum intensity ranged from about 1.05 to 1.38 °C, highest south of about 4°S and in the north-east (3–6°N, 128–132°E) and lowest east of Halmahera (Figure 3b). Mean duration (about 8–11 days) was longest in the north-east and the south-east (Figure 3c).

Frequency, intensity and duration therefore peak in different parts of the basin. The present data describe but cannot explain this mismatch. Plausible contributors are spatial differences in mixed-layer depth and stratification, surface heat flux, and advection through straits and around islands; the high-intensity band along the southern edge of the domain also borders the Banda Sea, where intensity was likewise highest in the southern basin [10]. Testing these explanations requires subsurface temperature, current and heat-budget data (Section 3.7).

The domain-mean frequency and duration are close to those reported for the waters south of West Java by [9] (1.99 events year^{-1} and 9 days over 1995–2024), although the two regions are more than 2,000 km apart and have contrasting oceanography. When intensity is measured against the climatology, as in [1], the Maluku Sea maximum intensity (1.20 °C) is also of the same order as in [9] (1.38 °C). Intensity measured against the threshold gives only 0.50 °C here because the threshold lies 0.72 °C above the climatology, so apparent differences between studies can arise from the intensity definition alone.

Baseline period, SST product (OISST here, OSTIA in [9]) and spatial resolution can also affect event metrics. The similarity in frequency and duration should therefore not be taken as evidence of common mechanisms.

3.2 Long-Term Trend in MHW Characteristics

Domain-mean MHW frequency increased significantly over the 30-year record (Theil–Sen slope +0.82 events year^{-1} decade^{-1}; modified Mann–Kendall p = 0.007; Figure 4). Annual frequency peaked at 5.17 events year^{-1} in both 2020 and 2021, with other high years in 1998 and 2010

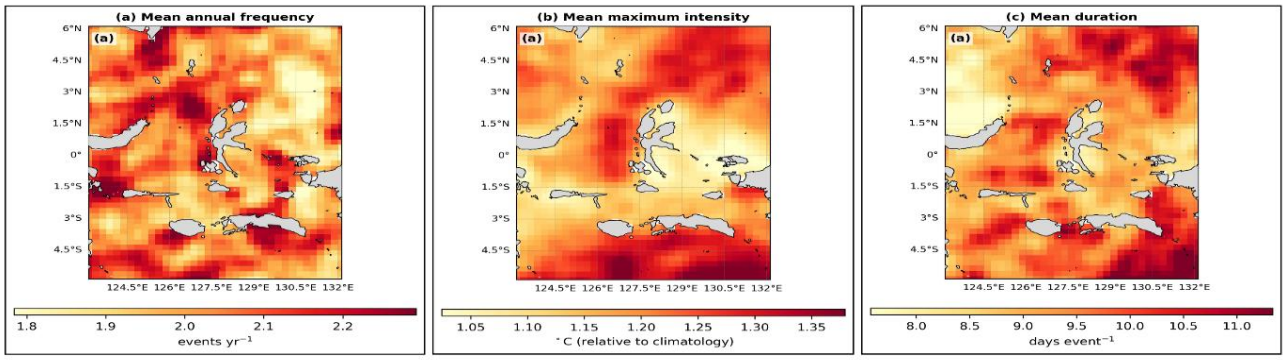


Figure 3. Mean spatial distribution of marine heatwave characteristics in the Maluku Sea, 1996-2025: (a) mean annual frequency (events year^{-1}), (b) mean maximum intensity (°C above threshold), and (c) mean duration (days)

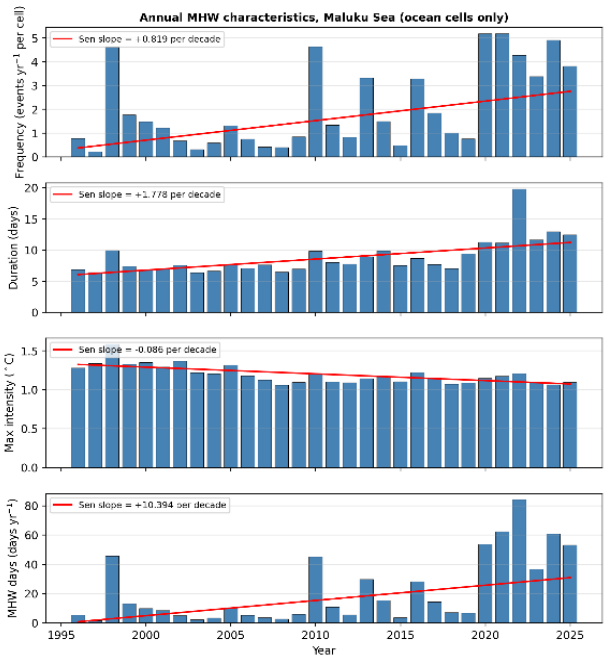


Figure 4. Annual time series of domain-averaged marine heatwave characteristics in the Maluku Sea, 1996-2025: (a) frequency, (b) maximum intensity, and (c) duration. Red bars indicate major ENSO extreme years.

(about 4.6), which coincide with the El Niño to La Niña transitions. MHW days also increased (+10.4 days year^{-1} decade^{-1}, p = 0.014) and reached 84 days in 2022. Autocorrelation correction matters: modified p-values exceeded the original ones (for example duration, 0.002 versus < 0.001; MHW days, 0.014 versus 0.002), yet all remain below 0.05. Domain-mean SST rose by 0.26 °C decade^{-1} (p < 0.001), so with a baseline equal to the study period the frequency and duration increases partly reflect background warming. Frequency trends were positive over most of the domain, strongest north of about 1.5°N and in the west-central basin (0°–3°S, 124°–127°E), and 848 of 1,711 ocean cells (50%) passed the FDR test (Figure 5a). Trends were weak and not significant in the south and east of Halmahera.

Maximum intensity decreased significantly (−0.086 °C decade^{-1}, p < 0.001; mean intensity −0.050 °C decade^{-1}, p < 0.001), but only 241 of 1,210 cells with sufficient data passed the FDR test, mainly in the north-west and south-west (Figure 5b). Duration increased (+1.78 days decade^{-1}, p = 0.002), with 394 of 1,211 cells passing FDR (Figure 5c). The annual maximum intensity showed no trend (−0.006 °C decade^{-1}, p = 0.94). Intensification therefore occurs through more numerous and longer events whose average peak amplitude is lower, while the strongest event of each year has not changed. A plausible, untested explanation is statistical: with a fixed baseline and rising SST, more days exceed the threshold by small margins, which lowers event-mean intensity metrics.

This differs from [10], who reported a frequency increase only (0.088 events year^{-1}, p = 0.010) in the Banda Sea, and from [9], who found no significant 30-year trend in any metric. Direct comparison is limited by differences in baseline, intensity definition and trend test: [10] used the original Mann–Kendall test and intensity relative to the threshold.

The significant intensity decline has not been reported in either study and cannot be attributed to a specific physical process here. Candidate explanations, such as a deepening mixed layer or stronger heat redistribution by the ITF [12], would require subsurface and transport data. The decline is therefore treated as an empirical result.

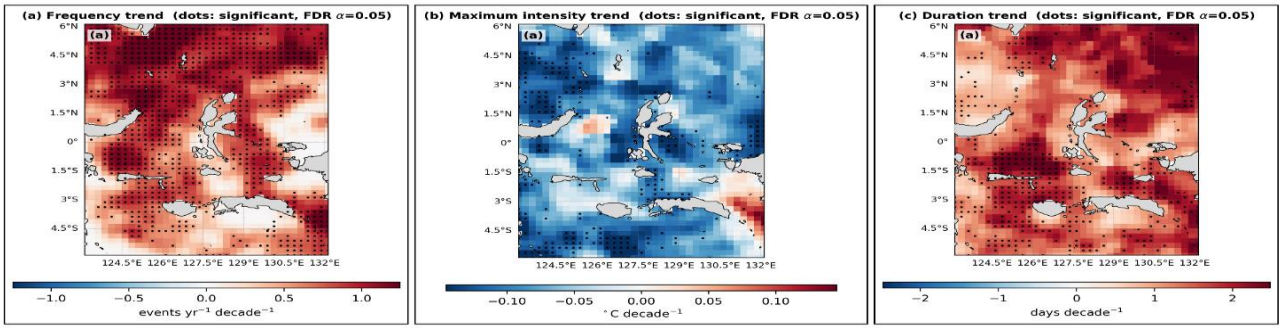


Figure 5. Theil–Sen trends of marine heatwave characteristics in the Maluku Sea, 1996–2025: (a) frequency (events year^{-1} decade^{-1}), (b) maximum intensity (°C decade^{-1}), (c) duration (days decade^{-1}). Dots mark cells significant after FDR control (α = 0.05).

DOI: 10.12962/inderaja.v20i2.10715

3.3 Association of ENSO with MHW Frequency

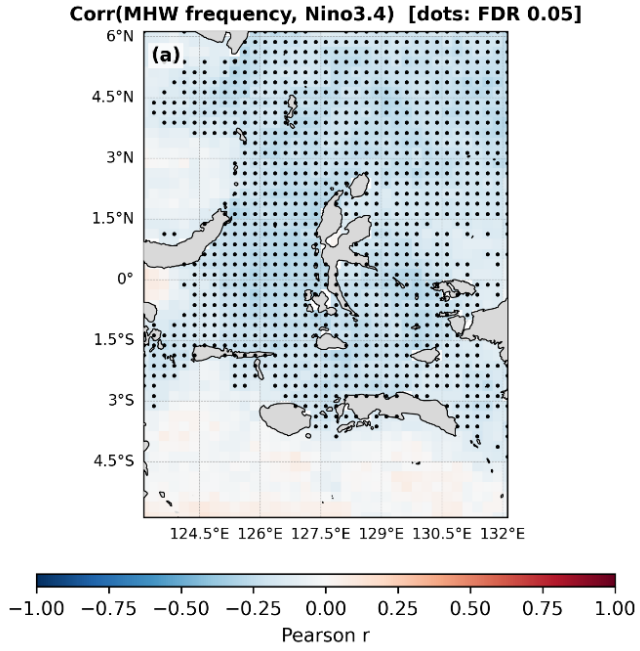


Figure 6. Correlation between monthly marine heatwave frequency anomalies and the Niño3.4 index in the Maluku Sea, 1996–2025 (detrended, lag 0). Dots mark cells significant after FDR control (α = 0.05, effective sample size).

The correlation between monthly MHW frequency anomalies and Niño3.4 (lag 0, detrended) was negative over nearly the whole basin but weak (range −0.31 to +0.12; Figure 6), and 1,085 of 1,715 ocean cells passed the FDR test, mainly north of about 3°S. Negative values mean more MHWs during La Niña. The composites agree (Figure 7): negative anomalies during El Niño (73 months), positive anomalies during La Niña (113 months) and weak anomalies in neutral months. In the domain mean, the La Niña anomaly was +0.087 events month^{-1} per cell (block-bootstrap p = 0.010), the El Niño anomaly −0.080 (p = 0.057) and the neutral anomaly −0.023 (p = 0.42). Individual cells in Figure 7 did not pass the FDR-controlled bootstrap test, so the spatial structure is indicative only.

At the domain scale, monthly MHW frequency anomalies were negatively correlated with Niño3.4 at lag 0 (r = −0.29, p = 0.002; N = 360, N_eff ≈ 112; detrended; without detrending r = −0.26, p = 0.011). The correlation weakened with lag (lag 1: r = −0.25, p = 0.009; lag 3: r = −0.11, p = 0.27) and no significant positive correlation appeared at lags 4–6 (lag 6: r = +0.14, p = 0.14). Using N = 360 instead of N_eff would give p < 0.001 at most lags and is over-optimistic. With seven lags tested, only lag 0 passes the Bonferroni threshold (p < 0.007). Controlling for the monsoon index at the same lag changed the result little (partial r = −0.28, p = 0.003). At the annual scale (n = 30) the association is suggestive but not conclusive: Pearson r = −0.26 (p = 0.20) and −0.36 after detrending (p = 0.06), with Spearman ρ = −0.37 (p = 0.042) after detrending.

In the Banda Sea [10] reported a weaker ENSO correlation (lag 0–1 month, r = −0.14; partial r = −0.08, p = 0.25). The

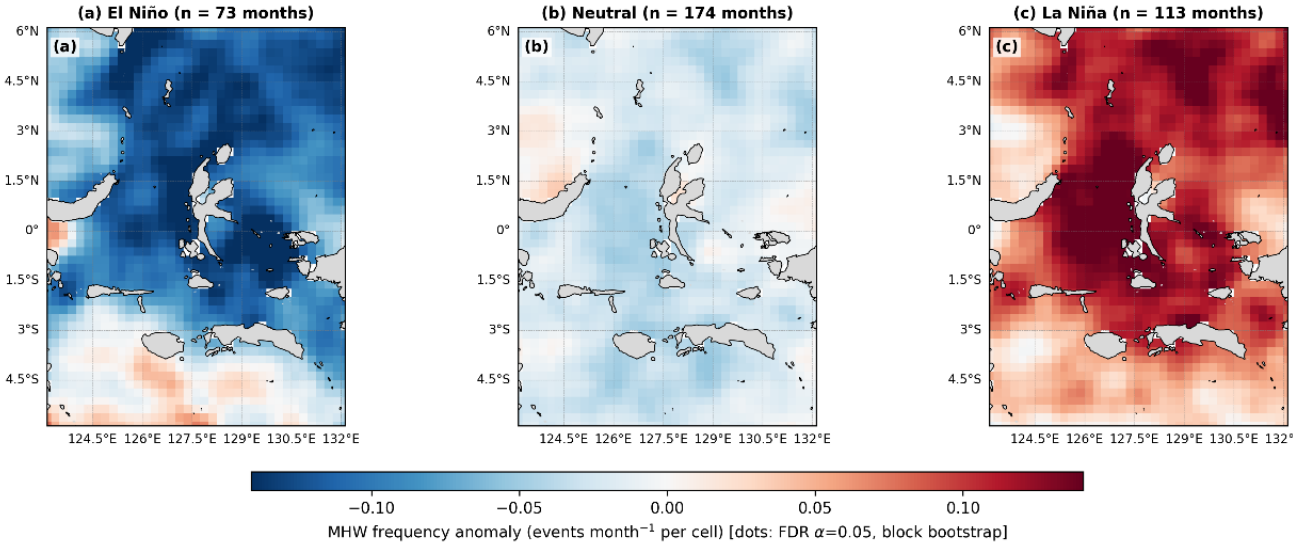


Figure 7. Composite anomalies of monthly marine heatwave frequency (events month^{-1} per cell) during (a) El Niño, (b) La Niña and (c) neutral months in the Maluku Sea, 1996–2025, classified with the ONI criterion.

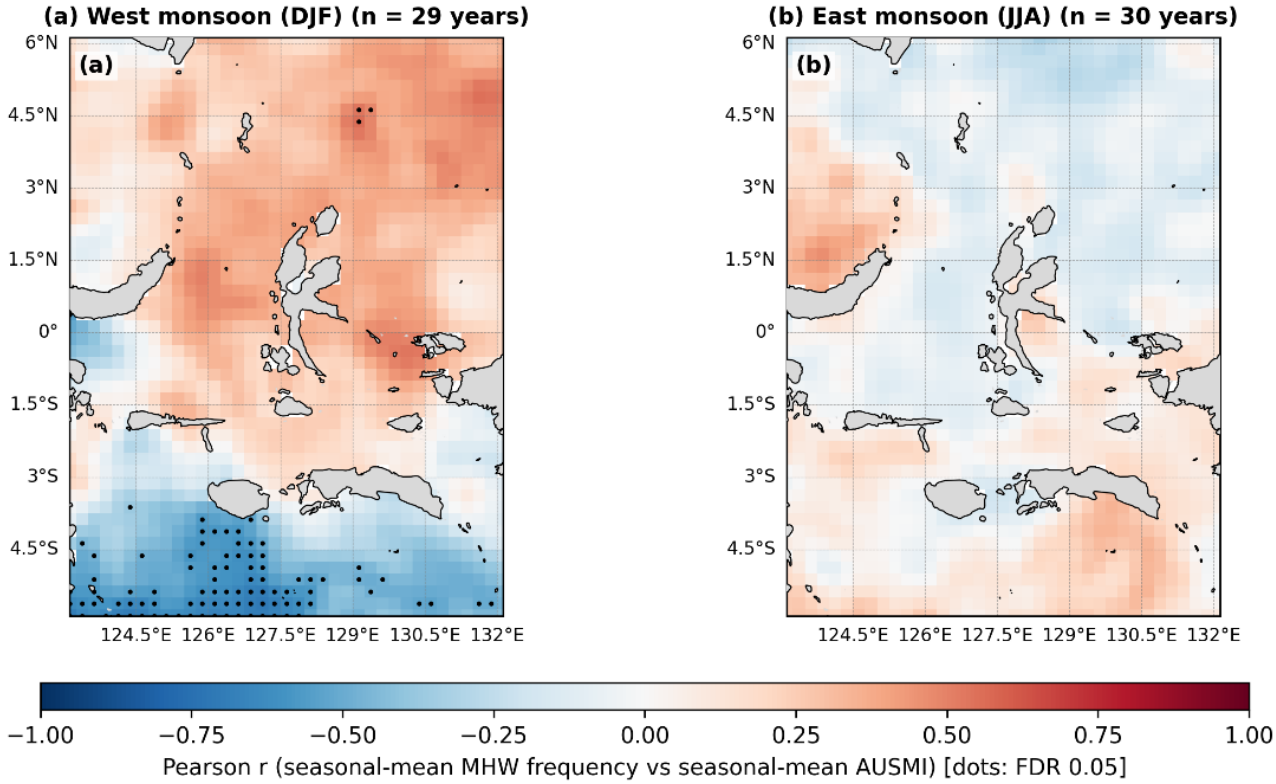


Figure 8. Correlation between seasonal-mean marine heatwave frequency and the seasonal-mean AUSMI in the Maluku Sea during (a) the west monsoon (DJF) and (b) the east monsoon (JJA), 1996–2025. Dots mark cells significant after FDR control (α = 0.05).

Maluku Sea value is larger and remains significant after controlling for the monsoon, but both are weak, the difference in r was not formally tested, and [10] did not use an effective sample size or detrending, so the comparison is only qualitative.

One hypothesis for the La Niña tendency is the position of the Maluku Sea near the northern entry of the ITF. ITF transport is reported to strengthen during La Niña and weaken during El Niño [32], [33], which could increase the advection of warm Pacific water into the basin, whereas the Banda Sea lies further downstream and is more strongly conditioned by local wind-driven upwelling and mixing [5]. This mechanism is consistent with the sign of the correlation but was not tested, because currents and ITF transport were not analyzed.

The result also nuances the common picture that El Niño is the main phase of anomalous warming in Indonesian seas through weaker trade winds and reduced upwelling [11], [32]. The La Niña tendency found here suggests that the response to ENSO is not spatially uniform across the Indonesian maritime continent.

3.4 Association of Monsoon Variability with MHW Frequency

Seasonal-mean AUSMI was only weakly correlated with seasonal-mean MHW frequency (Figure 8). In DJF (n = 29 years) correlations were mostly positive in the northern and central basin (r ≈ +0.2 to +0.5), but the 93 of 1,715 cells that passed FDR control lie in the south-west (about 3.5°–6°S, 124°–131°E), where r was negative (down to about −0.75). In JJA correlations were weak and of mixed sign, and no cell passed FDR control. The seasonal cycle shows slightly more MHW events per month in DJF (0.171 events month^{-1} per cell) than in JJA (0.150; Figure 9), but the difference is not significant (paired Wilcoxon p = 0.070). A seasonal reversal of the monsoon association is therefore not supported.

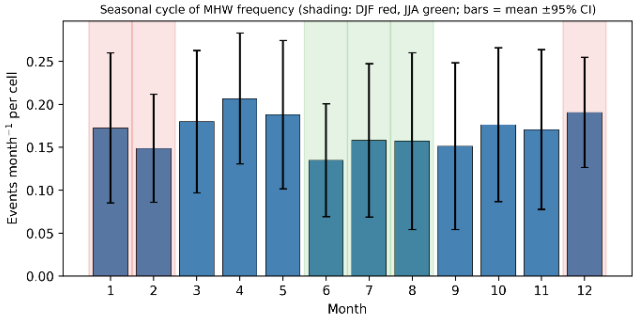


Figure 9. Seasonal cycle of domain-mean marine heatwave frequency (events month⁻¹ per cell) in the Maluku Sea, 1996–2025. Bars show monthly means with 95% confidence intervals; shading marks DJF (red) and JJA (green).

At the monthly scale, AUSMI anomalies were weakly associated with MHW frequency; the strongest correlation occurred at lag 6 (detrended r = −0.13, p = 0.015, N_eff ≈ 328), which does not pass the Bonferroni threshold and became weaker after controlling for ENSO (partial r = −0.10, p = 0.081; Table 2). In the multiple regression (lag 0), the ENSO coefficient was −0.069 events month⁻¹ per °C (HAC p = 0.002) and the monsoon coefficient −0.0014 (p = 0.79); the model explained 8.6% of the variance (R^2 = 0.086, adjusted R^2 = 0.081, F-test p = 0.003, N = 360, Durbin–Watson 0.99, which is why HAC errors were used). At the annual scale the monsoon correlation was positive but not significant (r = +0.25, p = 0.19; detrended +0.27, p = 0.15), although Spearman ρ = +0.43 (p = 0.019, detrended) hints at a rank relationship that needs testing with a more regionally appropriate index.

Table 2. Lagged and partial correlations of ENSO and monsoon variability with monthly MHW frequency anomalies in the Maluku Sea (1996–2025). Detrended series, N = 360 (N_eff ≈ 112 for ENSO and ≈ 328 for monsoon); partial correlation controls for the other index at the same lag.

Variable	Lag (month)	Lagged Correlation	Partial Correlation
ENSO	0	r = −0.293, p = 0.002	r = −0.283, p = 0.003
Monsoon	6	r = −0.135, p = 0.015	r = −0.097, p = 0.081

The weak monthly, seasonal and annual associations (Table 2, Figure 8) contrast with [10], where the monsoon index dominated in the Banda Sea (r = 0.58; partial r = 0.55). Differences in index construction, statistical treatment (no N_eff or detrending in [10]) and location limit the comparison. The AUSMI domain lies largely south of the equator, whereas the Maluku Sea spans 6°S–6°N, so the index may not represent wind variability over the whole study area.

Enhanced vertical mixing and upwelling under the south-east monsoon winds, which cool the surface [8], [11], [34], is physically plausible and would favor fewer MHWs in JJA. The present data do not confirm it: the DJF–JJA difference is not significant and no stratification or subsurface data were analyzed. The monsoon role is

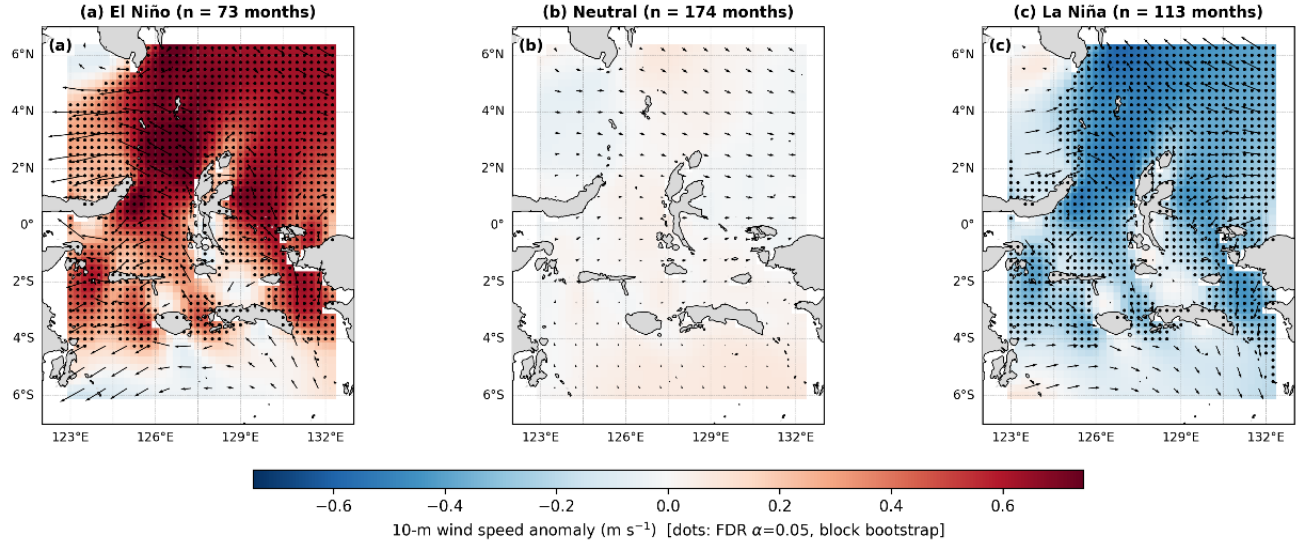


Figure 10. ENSO composite of 10-m wind speed anomaly (m s⁻¹) in the Maluku Sea during 1996–2025 for (a) El Niño (n = 73 months), (b) Neutral (n = 174 months), and (c) La Niña (n = 113 months).

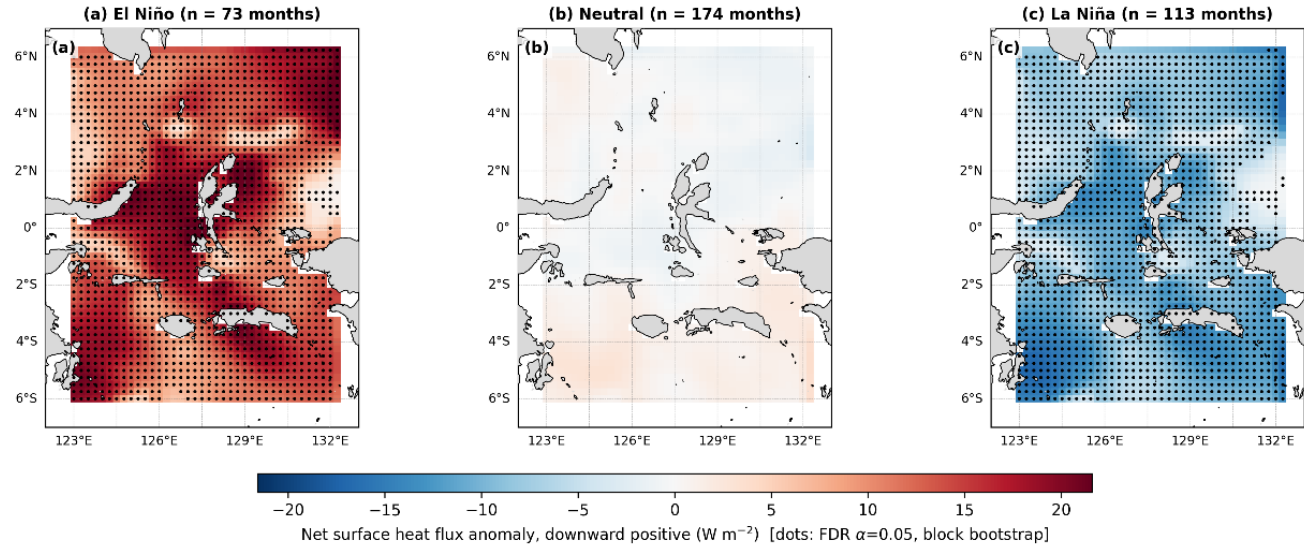


Figure 11. ENSO composite of net surface heat flux anomaly (Qnet, W m^{-2}) in the Maluku Sea during 1996–2025 for (a) El Niño (n = 73 months), (b) Neutral (n = 174 months), and (c) La Niña (n = 113 months).

therefore regarded as not demonstrated with this index, not as negligible.

3.5 ENSO Composite of 10-m Wind Speed Anomaly

ENSO composites of 10-m wind speed anomalies (Figure 10) give area-mean anomalies of +0.37 m s^{-1} during El Niño (n = 73 months) and −0.26 m s^{-1} during La Niña (n = 113), both significant (block-bootstrap p = 0.001), and near zero in neutral months (+0.01 m s^{-1}, p = 0.85). Monthly wind-speed anomalies correlated negatively with MHW frequency anomalies (r = −0.48, p < 0.001, N_eff ≈ 220) and positively with Niño3.4 (r = +0.41). Weaker winds, which tend to occur during La Niña, thus coincide with more MHWs. Weaker winds reduce vertical mixing and turbulent heat loss and favor shallow warm surface layers [35]–[37], which is consistent with this correlation. The wind–MHW correlation is not corrected for the shared dependence on ENSO, so it does not by itself establish a wind effect.

The wind composites thus show a clear ENSO signal in near-surface winds, with the La Niña wind reduction being the atmospheric feature most strongly associated with MHW frequency in the variables examined. Its effect on evaporation is assessed in Section 3.6.

3.6 ENSO Composite of Net Surface Heat Flux Anomaly

ENSO composites of net surface heat flux (Qnet, positive downward; Figure 11) give area-mean anomalies of +13.4 W m^{-2} during El Niño and −9.1 W m^{-2} during La Niña (both p = 0.001), and +0.3 W m^{-2} in neutral months (p = 0.90). Absolute magnitudes depend on the ERA5 sampling and unit conversion, so the sign and relative size of the anomalies are emphasized.

Shortwave radiation (SSR) dominates the Qnet anomaly (+16.4 W m^{-2} in El Niño, −8.8 W m^{-2} in La Niña). Longwave radiation (−2.7 and +0.9 W m^{-2}), sensible heat (+0.6 and −0.8 W m^{-2}) and latent heat (−0.9 and −0.4 W m^{-2}, not significant, p = 0.42 and 0.65) are smaller. La Niña therefore brings less incoming shortwave radiation, which is consistent with greater cloudiness, and no detectable change in evaporative loss in the composite. Cloud-related shortwave anomalies have likewise been linked to MHW conditions in other marginal seas [38].

The key result is that MHW frequency is higher during La Niña although Qnet is lower. Monthly Qnet anomalies are not significantly correlated with MHW frequency (r = −0.08, p = 0.22), and SSR is negatively correlated (r = −0.21, p = 0.003): MHWs coincide with reduced, not enhanced, shortwave input. Longwave (r = +0.24, p = 0.001) and latent heat flux (r = +0.17, p = 0.004) correlate

positively, meaning that smaller radiative and evaporative heat loss accompanies MHWs, but these associations are weak. Local surface heat gain therefore does not explain the La Niña tendency. Reduced wind-driven mixing and oceanic heat advection, including the ITF response to La Niña [32], [33], remain hypotheses that these data cannot test.

Together, the wind and heat flux results show that the ENSO–MHW association is not explained by local net heat gain, and that reduced winds are the atmospheric variable most closely associated with MHW frequency. A mixed-layer heat budget with ocean currents, sea level and Argo profiles is needed to separate the contributions.

3.7 Synthesis and Study Limitations

ENSO shows a stronger statistical association with MHW frequency than the monsoon index used here, with more MHWs during La Niña. The association is weak: ENSO and monsoon together explain 8.6% of the variance in monthly MHW frequency anomalies, so more than 90% remains unexplained and is likely governed by local ocean dynamics, other climate modes and stochastic atmospheric variability. The annual-scale association is not significant under Pearson correlation, and ENSO should not be used as a predictor of MHW occurrence without further testing.

The increase in MHW frequency and duration together with a decline in event maximum intensity is a long-term shift in MHW characteristics relative to the 1996–2025 baseline. No change-point analysis was applied, and the shift partly reflects the 0.26 °C decade^{-1} SST warming of the domain.

Several limitations apply. (1) The baseline equals the study period, and a 1982–2011 baseline sensitivity test is still needed. (2) The AUSMI is defined mostly south of the study area and may not represent local monsoon winds; the monsoon result is specific to this index. (3) The Indian Ocean Dipole (IOD), which modulates Indonesian SST and ITF transport [32], [39], [40] and often co-occurs with ENSO, was not analyzed, so part of the ENSO association may include IOD effects; adding the Dipole Mode Index is a priority. (4) Air–sea fluxes were examined only as composites, and ocean currents, sea level, ITF transport and subsurface temperature were not analyzed, so physical mechanisms cannot be established. (5) The 0.25° OISST resolution may not resolve strait and coastal processes. (6) The ERA5 flux magnitudes depend on sampling and unit conversion. (7) Monthly MHW frequency is skewed and zero-inflated, which affects Pearson assumptions, and seven lags were tested per index. (8) All relationships are associations and not proof of causation.

IV. CONCLUSION

This study documents a long-term shift in marine heatwave (MHW) characteristics in the Maluku Sea over the past three decades. MHW frequency and duration increased significantly, particularly in the northern and central basin, while event maximum intensity decreased. These changes are relative to a 1996–2025 baseline and partly reflect the 0.26 °C decade^{-1} warming of the basin.

ENSO shows a stronger statistical association with MHW frequency than the monsoon variability examined, with more MHWs during La Niña, whereas the monsoon association is not significant after controlling for ENSO. The associations are weak (R^2 = 0.086), and the Indian Ocean Dipole and ocean dynamics were not analyzed, so causal attribution is not possible. La Niña conditions may nevertheless be a useful, though not sufficient, indicator for marine heat stress outlooks in Eastern Indonesia.

ACKNOWLEDGEMENT

The author gratefully acknowledges the National Oceanic and Atmospheric Administration (NOAA) for providing the Optimum Interpolation Sea Surface Temperature (OISST) Version 2.1 dataset and the Niño 3.4 sea surface temperature anomaly data used in this study. The author also acknowledges the Copernicus Climate Change Service (C3S) for providing the ERA5 reanalysis dataset, including the 10-m wind and surface heat flux variables. The author expresses sincere gratitude to the supervisors for their invaluable guidance, constructive feedback, and continuous encouragement throughout this research. Appreciation is also extended to the Sekolah Tinggi Meteorologi Klimatologi dan Geofisika (STMKG) for providing academic support and a conducive environment for conducting this research. Finally, the author would like to thank all colleagues and individuals whose valuable discussions, suggestions, and support contributed to the successful completion of this study.

REFERENCES

[1] A. J. Hobday *et al.*, “A hierarchical approach to defining marine heatwaves,” *Prog. Oceanogr.*, vol. 141, pp. 227–238, 2016, doi: 10.1016/j.pocean.2015.12.014.
[2] E. C. J. Oliver *et al.*, “Longer and more frequent marine heatwaves over the past century,” *Nat. Commun.*, vol. 9, Art. no. 1324, Dec. 2018, doi: 10.1038/s41467-018-03732-9.
[3] F. Tan *et al.*, “El Niño was a key driver of anomalous ocean warming in Southeast Asia in 2023,” *Sci. Rep.*, vol. 15, no. 1, Dec. 2025, doi: 10.1038/s41598-025-99511-w.
[4] H. A. Scannell, A. J. Pershing, M. A. Alexander, A. C. Thomas, and K. E. Mills, “Frequency of marine heatwaves in

the North Atlantic and North Pacific since 1950," *Geophys. Res. Lett.*, vol. 43, no. 5, pp. 2069–2076, Mar. 2016, doi: 10.1002/2015GL067308.

[5] J. Sprintall *et al.*, "The Indonesian seas and their role in the coupled ocean–climate system," *Nat. Geosci.*, vol. 7, no. 7, pp. 487–492, 2014, doi: 10.1038/ngeo2188.

[6] A. L. Gordon, R. D. Susanto, and A. Ffield, "Throughflow within Makassar Strait," *Geophys. Res. Lett.*, vol. 26, no. 21, pp. 3325–3328, Nov. 1999, doi: 10.1029/1999GL002340.

[7] T. Zhang, W. Wang, Q. Xie, and L. Chen, "Heat contribution of the Indonesian throughflow to the Indian Ocean," *Acta Oceanol. Sin.*, vol. 38, no. 4, pp. 72–79, 2019, doi: 10.1007/s13131-019-1414-6.

[8] F. A. Schott and J. P. McCreary, "The monsoon circulation of the Indian Ocean," *Prog. Oceanogr.*, vol. 51, no. 1, pp. 1–123, 2001, doi: 10.1016/S0079-6611(01)00083-0.

[9] A. A. Riztiawan *et al.*, "Karakteristik gelombang panas laut di perairan selatan Jawa Barat," *J. Kelaut. Indones. J. Mar. Sci. Technol.*, vol. 18, no. 3, pp. 218–226, Dec. 2025, doi: 10.21107/jk.v18i3.31731.

[10] M. D. Alkhaiy and A. S. Al-Mubarak, "Relative roles of monsoon and ENSO in driving marine heatwaves in the Banda Sea, over the period 2005–2024," SSRN preprint, 2026. [Online]. Available: https://ssrn.com/abstract=6669095

[11] R. D. Susanto, A. L. Gordon, and Q. Zheng, "Upwelling along the coasts of Java and Sumatra and its relation to ENSO," *Geophys. Res. Lett.*, vol. 28, no. 8, pp. 1599–1602, Apr. 2001, doi: 10.1029/2000GL011844.

[12] S. Hu and J. Sprintall, "Observed strengthening of interbasin exchange via the Indonesian seas due to rainfall intensification," *Geophys. Res. Lett.*, vol. 44, no. 3, pp. 1448–1456, Feb. 2017, doi: 10.1002/2016GL072494.

[13] R. D. Susanto and Y. T. Song, "Indonesian throughflow proxy from satellite altimeters and gravimeters," *J. Geophys. Res. Oceans*, vol. 120, no. 4, pp. 2844–2855, Apr. 2015, doi: 10.1002/2014JC010382.

[14] B. Wang *et al.*, "Fundamental challenge in simulation and prediction of summer monsoon rainfall," *Geophys. Res. Lett.*, vol. 32, no. 15, Aug. 2005, doi: 10.1029/2005GL022734.

[15] B. Huang *et al.*, "Improvements of the daily optimum interpolation sea surface temperature (DOISST) version 2.1," *J. Clim.*, vol. 34, no. 8, pp. 2923–2939, 2021, doi: 10.1175/JCLI-D-20-0166.1.

[16] R. W. Reynolds, T. M. Smith, C. Liu, D. B. Chelton, K. S. Casey, and M. G. Schlax, "Daily high-resolution-blended analyses for sea surface temperature," *J. Clim.*, vol. 20, no. 22, pp. 5473–5496, 2007, doi: 10.1175/2007JCLI1824.1.

[17] V. Banzon, T. M. Smith, T. M. Chin, C. Liu, and W. Hankins, "A long-term record of blended satellite and in situ sea-surface temperature for climate monitoring, modeling and environmental studies," *Earth Syst. Sci. Data*, vol. 8, no. 1, pp. 165–176, 2016, doi: 10.5194/essd-8-165-2016.

[18] World Meteorological Organization, "WMO guidelines on the calculation of climate normals," WMO-No. 1203, Geneva, Switzerland, 2017. Accessed: Jun. 20, 2026. [Online]. Available: https://library.wmo.int/records/item/55797-wmo-guidelines-on-the-calculation-of-climate-normals

[19] Y. Kajikawa, B. Wang, and J. Yang, "A multi-time scale Australian monsoon index," *Int. J. Climatol.*, vol. 30, no. 8, pp. 1114–1120, 2010, doi: 10.1002/joc.1955.

[20] H. Hersbach *et al.*, "The ERA5 global reanalysis," *Q. J. R. Meteorol. Soc.*, vol. 146, no. 730, pp. 1999–2049, 2020, doi: 10.1002/qj.3803.

[21] A. J. Hobday *et al.*, "Categorizing and naming marine heatwaves," *Oceanography*, vol. 31, no. 2, pp. 162–173, 2018, doi: 10.5670/oceanog.2018.205.

[22] S. Darmaraki *et al.*, "Future evolution of marine heatwaves in the Mediterranean Sea," *Clim. Dyn.*, vol. 53, no. 3–4, pp. 1371–1392, Aug. 2019, doi: 10.1007/s00382-019-04661-z.

[23] K. H. Hamed and A. R. Rao, "A modified Mann–Kendall trend test for autocorrelated data," *J. Hydrol.*, vol. 204, no. 1–4, pp. 182–196, 1998, doi: 10.1016/S0022-1694(97)00125-X.

[24] H. B. Mann, "Nonparametric tests against trend," *Econometrica*, vol. 13, no. 3, pp. 245–259, 1945, doi: 10.2307/1907187.

[25] M. G. Kendall, *Rank Correlation Methods*, 4th ed. London, U.K.: Charles Griffin, 1975.

[26] P. K. Sen, "Estimates of the regression coefficient based on Kendall's tau," *J. Am. Stat. Assoc.*, vol. 63, no. 324, pp. 1379–1389, Dec. 1968, doi: 10.1080/01621459.1968.10480934.

[27] Y. Benjamini and Y. Hochberg, "Controlling the false discovery rate: A practical and powerful approach to multiple testing," *J. R. Stat. Soc. B*, vol. 57, no. 1, pp. 289–300, 1995, doi: 10.1111/j.2517-6161.1995.tb02031.x.

[28] D. S. Wilks, *Statistical Methods in the Atmospheric Sciences*, 3rd ed. Amsterdam, The Netherlands: Academic Press, 2011.

[29] C. S. Bretherton, M. Widmann, V. P. Dymnikov, J. M. Wallace, and I. Bladé, "The effective number of spatial degrees of freedom of a time-varying field," *J. Clim.*, vol. 12, no. 7, pp. 1990–2009, 1999, doi: 10.1175/1520-0442(1999)012<1990:TENOSD>2.0.CO;2.

[30] W. K. Newey and K. D. West, "A simple, positive semi-definite, heteroskedasticity and autocorrelation consistent covariance matrix," *Econometrica*, vol. 55, no. 3, pp. 703–708, 1987, doi: 10.2307/1913610.

[31] K. A. McKinnon, A. Rhines, M. P. Tingley, and P. Huybers, "The changing shape of Northern Hemisphere summer temperature distributions," *J. Geophys. Res. Atmos.*, vol. 121, no. 15, pp. 8849–8868, 2016, doi: 10.1002/2016JD025292.

[32] A. Li, Y. Zhang, M. Hong, J. Shi, and J. Wang, "Relative importance of ENSO and IOD on interannual variability of Indonesian Throughflow transport," *Front. Mar. Sci.*, vol. 10, 2023, doi: 10.3389/fmars.2023.1182255.

[33] G. Meyers, "Variation of Indonesian throughflow and the El Niño–Southern Oscillation," *J. Geophys. Res.*, vol. 101, no. C5, pp. 12255–12263, 1996, doi: 10.1029/95JC03729.

[34] C.-P. Chang, Z. Wang, J. McBride, and C.-H. Liu, "Annual cycle of Southeast Asia–Maritime Continent rainfall and the asymmetric monsoon transition," *J. Clim.*, vol. 18, no. 2, pp. 287–301, 2005.

[35] C. W. Fairall, E. F. Bradley, J. E. Hare, A. A. Grachev, and J. B. Edson, "Bulk parameterization of air–sea fluxes: Updates and verification for the COARE algorithm," *J. Clim.*, vol. 16, no. 4, pp. 571–591, 2003.

[36]G. Bonino *et al.*, "Mediterranean summer marine heatwaves triggered by weaker winds under subtropical ridges," *Nat. Geosci.*, vol. 18, no. 9, pp. 848–853, Sep. 2025, doi: 10.1038/s41561-025-01762-9.

[37]A. Schaeffer and M. Roughan, "Subsurface intensification of marine heatwaves off southeastern Australia: The role of stratification and local winds," *Geophys. Res. Lett.*, vol. 44, no. 10, pp. 5025–5033, May 2017, doi: 10.1002/2017GL073714.

[38]W. Choi, M. Bang, Y. Joh, Y. G. Ham, N. Kang, and C. J. Jang, "Characteristics and mechanisms of marine heatwaves in the East Asian marginal seas: Regional and seasonal differences," *Remote Sens.*, vol. 14, no. 15, Art. no. 3522, Aug. 2022, doi: 10.3390/rs14153522.

[39]D. Yuan, H. Zhou, and X. Zhao, "Interannual climate variability over the tropical Pacific Ocean induced by the Indian Ocean Dipole through the Indonesian Throughflow," *J. Clim.*, vol. 26, no. 9, pp. 2845–2861, 2013, doi: 10.1175/JCLI-D-12-00117.1.

[40]N. H. Saji, B. N. Goswami, P. N. Vinayachandran, and T. Yamagata, "A dipole mode in the tropical Indian Ocean," *Nature*, vol. 401, pp. 360–363, 1999, doi: 10.1038/43854.



Creative Commons Attribution-NonCommercial-ShareAlike 4.0 International (CC BY-NC-SA 4.0)